



ELSEVIER

Spectrochimica Acta Part B 56 (2001) 851–864

SPECTROCHIMICA
ACTA
PART B

www.elsevier.nl/locate/sab

On-line analysis of ambient air aerosols using laser-induced breakdown spectroscopy[☆]

J.E. Carranza, B.T. Fisher, G.D. Yoder, D.W. Hahn*

Department of Mechanical Engineering, P.O. Box 116300, University of Florida, Gainesville, FL 32611, USA

Received 12 October 2000; accepted 1 March 2001

Abstract

Laser-induced breakdown spectroscopy is developed for the detection of aerosols in ambient air, including quantitative mass concentration measurements and size/composition measurements of individual aerosol particles. Data are reported for ambient air aerosols containing aluminum, calcium, magnesium and sodium for a 6-week sampling period spanning the Fourth of July holiday period. Measured mass concentrations for these four elements ranged from 1.7 parts per trillion (by mass) to 1.7 parts per billion. Ambient air concentrations of magnesium and aluminum revealed significant increases during the holiday period, which are concluded to arise from the discharge of fireworks in the lower atmosphere. Real-time conditional data analysis yielded increases in analyte spectral intensity approaching 3 orders of magnitude. Analysis of single particles yielded composition-based aerosol size distributions, with measured aerosol diameters ranging from 100 nm to 2 μm . The absolute mass detection limits for single particle analysis exceeded sub-femtogram values for calcium-containing particles, and was on the order of 2–3 femtograms for magnesium and sodium-based particles. Overall, LIBS-based analysis of ambient air aerosols is a promising technique for the challenging issues associated with the real-time collection and analysis of ambient air particulate matter data. © 2001 Elsevier Science B.V. All rights reserved.

Keywords: Laser-induced breakdown spectroscopy (LIBS); Aerosol; Particulate matter

[☆]This paper was presented at the 1st International Congress on Laser Induced Plasma Spectroscopy and Applications, Pisa, Italy, October 2000, and is published in the Special Issue of *Spectrochimica Acta Part B*, dedicated to that conference.

*Corresponding author. Tel.: +1-352-392-0807; fax: +1-352-392-1071.

E-mail address: dwhahn@ufl.edu (D.W. Hahn).

1. Introduction

The development of techniques for the on-line analysis of single aerosol particles has been an active area of research in recent years. As discussed in the introduction to a collection of papers focusing on single particle analysis, recent efforts have examined: inlet design and particle transport; detection schemes including mass spectrometry and emission spectroscopy; instrument portability and field deployment; and environmental applications [1]. Environmental applications of single aerosol particle analysis techniques are of particular interest given the recent recognition of the detrimental impacts of ambient air particulate matter (PM) on human health. The United States Environmental Protection Agency (EPA) concluded in 1996 that particulate matter is associated with increased morbidity and mortality [2]. In recent years, a number of international studies have corroborated the conclusion that health risks are associated with ambient air particulate matter. In response to these health risk factors, research agendas have targeted a number of program areas including: measures of outdoor PM and associated human exposures; characterization of emissions sources; air quality model development and testing; and assessment of hazardous PM components [3]. The need for ambient air particulate matter data, specifically size and composition measurements of individual particles, is common to all of these research areas. This need for PM data combined with the development of advanced aerosol analysis techniques has served as a motivation for the development of on-line or real-time aerosol particle analyzers. Such methods have the potential to provide the time-resolved particle size and composition data required for PM analyses in a cost-effective and timely manner.

The majority of development work for on-line particle analysis relies on mass spectrometry or atomic emission spectroscopy as the analytical method for particle composition measurements. Particle size may be inferred directly from the mass of the particle's constituent elements or recorded by auxiliary measurements such as particle mobility analysis or aerodynamic sizing. Re-

search groups have employed various combinations of these analytical methods, thereby realizing several approaches to on-line analysis of particle size and composition. Implementations include, for example: aerodynamic sizing via particle time-of-flight coupled with laser-desorption/mass spectrometry [4,5]; differential mobility sizing coupled with laser-desorption/mass spectrometry [6]; differential mobility sizing coupled with thermal-desorption/mass spectrometry [7] and direct elemental mass and composition using laser atomization/mass spectrometry [8]; or laser-induced breakdown spectroscopy [9]. In addition, several techniques based on microwave or inductively coupled plasma atomic emission spectrometry are readily implemented for real-time analysis of PM mass concentrations [10–13], but generally are not amendable to single-particle analysis. This paper will focus on laser-induced breakdown spectroscopy, referred to as LIBS, which utilizes atomic emission spectroscopy for the analysis of atomic species present in an individual aerosol particle. The LIBS technique can yield quantitative measurements of the mass of constituent elements, thereby enabling a direct measurement of size and composition of individual particles.

LIBS, also referred to as laser-induced plasma spectroscopy, uses a laser-induced microplasma to vaporize and dissociate all molecules and fine particles within the sample volume. Atoms within the plasma are subsequently excited within the energetic plasma, resulting in atomic emission. The technique of laser-induced plasma spectroscopy dates to the 1960s and has been applied to the analysis of solids, liquids and gases. A number of literature reviews are available that cover a wide range of LIBS-based analyses [14–18]. Relevant to ambient air particulate matter, several recent review papers have focused specifically on the use of LIBS for aerosol measurements and environmental monitoring [19,20]. The LIBS technique has been applied to environmental and industrial process monitoring by a number of research groups [21–27].

Most elements targeted for emissions monitoring (e.g. toxic metals) exist as particulates, with the exception of metal vapors in very high-tem-

perature combustion chambers. Mercury is a noted exception under many high to moderate temperature conditions. The presence of discrete particles is significant when utilizing an essentially point-sampling technique as realized with LIBS. For example, traditional ensemble-averaging of LIBS spectra may limit signal-to-noise ratios of targeted analytes if the overall sampling rate of the analyte-containing particles is low. In response to such issues, several approaches have been formulated to enhance the sensitivity of the LIBS technique by examining individual spectra, with goals of rejecting spectra that are irregular, or more significantly, lacking the analyte signal of interest [23,28]. The use of a suitable conditional analysis algorithm can yield significant increases in signal-to-noise ratios, but more importantly, opens the door to the analysis of single-shot LIBS spectra that correspond to individual aerosol particles. The basis of LIBS for the analysis of discrete aerosol particles was developed in earlier publications [9,29], including LIBS-based analysis of different aerosol particle types under a range of well-controlled experimental conditions. The goals of this paper are to further characterize the use of LIBS for the direct monitoring of ambient air aerosols.

2. Experimental

2.1. LIBS system

The LIBS system has been described in an earlier publication [9], hence only a brief overview of the system will be presented. The laser-induced plasma was generated using a Q-switched Nd:YAG laser at the fundamental frequency, with a 10-ns pulse width, 375-mJ pulse energy and a 5-Hz pulse repetition rate. The expanded laser beam (12-mm diameter) was focused in the sample chamber using a 75-mm UV grade lens (50-mm diameter). The plasma emission was collected along the direction of the incident beam and separated using a pierced mirror. The plasma emission was fiber-coupled to a 0.275-m spectrometer, dispersed with a 2400-groove/mm grating (0.03 nm/pixel, 120-pm resolution), and

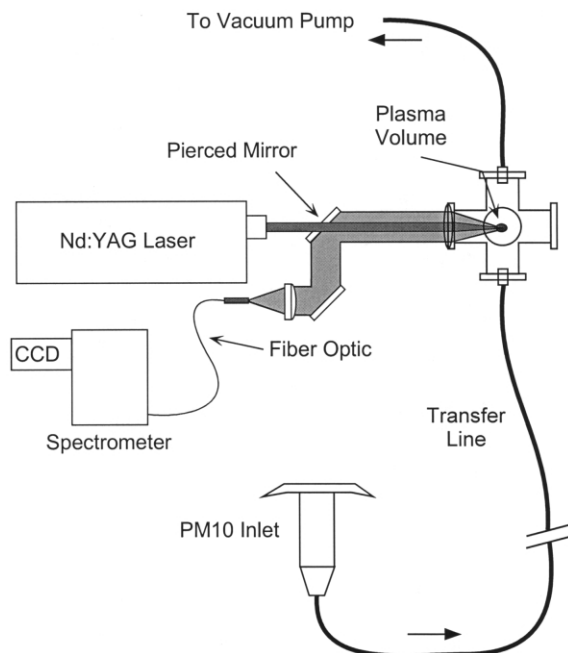


Fig. 1. Schematic of ambient air sampling system. The system includes a standard PM10 inlet to remove particles greater than 10 μm in diameter.

recorded with an intensified, charge-coupled device (iCCD) detector array. Signal integration was performed using delay times ranging from 30 to 40 μs with respect to the incident laser pulse, and integration times ranging from 40 to 150 μs , which were selected to optimize the signal-to-noise ratios of the analyte emission peaks. Plasma temperatures were on the order of 10000 K during these temporal windows, as measured using a Boltzmann plot based on 21 chromium I emission lines.

2.2. Aerosol sampling system

An ambient air sampling system was designed to bring a well-controlled flow of ambient air to the prototype LIBS instrument. A schematic of the overall experimental system is depicted in Fig. 1. A US EPA standard PM10 inlet was utilized at the air inlet of the sample line. A PM10 inlet removes all particles greater than 10 μm in diameter via inertial impaction, while also ensuring uniform sampling of air. The air was drawn into

the PM10 inlet at a volumetric flow rate of 16.7 liters/min ($\sim 1 \text{ m}^3/\text{h}$), and subsequently transferred to the LIBS sample chamber using 12-mm inner diameter stainless steel tubing. The sampling inlet was located on the roof of a single story building adjacent to the second story laboratory housing the LIBS system. The inlet was positioned approximately 1 m from the edge of the roof and approximately 3 m from the laboratory. The inlet was positioned to be as free as possible from any obstructions; however, no detailed analysis of building interactions with ambient air sampling was included for this study. The stainless steel transfer line was connected directly to the inlet of the sample chamber, where the airflow subsequently entered a six-way stainless-steel vacuum cross. A vacuum pump was connected to the outlet of the sample chamber, and was used to maintain the overall sampling rate. The pressure in the sample chamber was maintained at 1 torr below atmospheric pressure. An aerosol deposition program [30] was used to calculate the particle transfer efficiency throughout the entire sampling system. The transport efficiency from the sampling inlet to the LIBS sample chamber as a function of particle diameter is presented in Fig. 2. The efficiencies ranged from 92 to 99% for particulate diameters between 0.1 and 2.5 μm . Essentially all particle diameters reported in this study ranged between 0.1 and 1.0 μm , with corresponding transport efficiency between 97 and 99%. In consideration of these calculations, no corrections were made to particle size distributions or particle mass concentrations based on the aerosol transport efficiency.

2.3. Ambient air monitoring

Ambient air was monitored on the University of Florida campus using the LIBS technique between Monday, June 28, 2000 and Friday, July 7, 2000, and again between Tuesday, August 1, 2000 and Friday, August 5, 2000. These sample windows were selected to overlap with the Fourth of July holiday period, a holiday associated with the use of fireworks. Specifically, there were at least five municipal fireworks displays within a 50-mile radius of the University of Florida

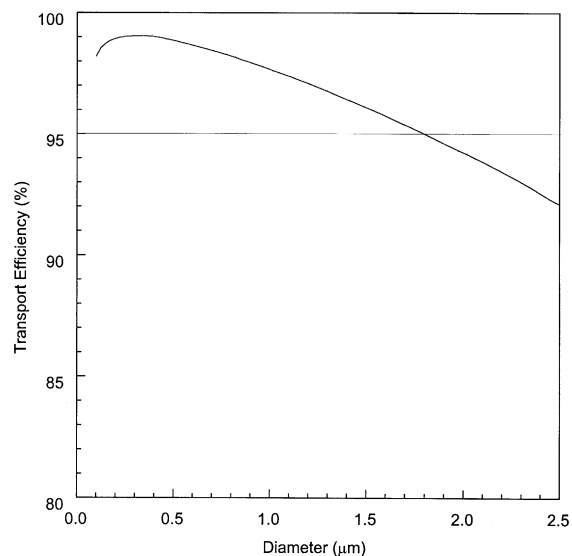


Fig. 2. Transport efficiency of ambient air particles from the inlet to the LIBS sample chamber as a function of the particle diameter.

between July 3 and July 4 (Tuesday). In addition, the use of fireworks by individual persons is legal in many areas surrounding the campus; therefore the discharge of fireworks was expected to be concentrated between Saturday July 1 and July 4, as attributed to both individual usage and municipal displays. LIBS data were collected typically twice each day, generally in the morning hours and in the afternoon/evening hours. During each sampling period, spectral data were collected for approximately 2 h. During the course of experiments, daily high temperatures ranged from 28 to 34°C, overnight low temperatures ranged from 18 to 23°C, and daily wind speeds ranged from 0 to 13 mph, with winds primarily to the north direction. Rain was periodic (maximum of 2.4 cm on June 29) during the nearly 3 weeks of sampling; however, no data were recorded during periods of rain.

2.4. LIBS data analysis

Ambient air mass concentration measurements of the targeted elements were recorded using a conditional data analysis scheme. During each nominally 2-h sampling period, spectra were

recorded using 1200-shot pulse sequences, which corresponds to a 4-min sample for the 5-Hz laser repetition rate. For each spectral window, between 8 and 14 1200-shot sequences were recorded, corresponding to a total of between 9600 and 16 800 laser pulses for each reported analyte mass concentration. Spectra that contained significant emission intensity for a targeted analyte species were identified as particle hits. For each LIBS spectrum, the emission intensity about the expected analyte peak was compared to the emission intensity of an adjacent, featureless continuum spectral region. The spectrum was classified as a particle hit if the ratio of emission intensities exceeded a threshold value, typically 75–150% above the nominal ratio corresponding to the absence of any analyte emission line intensity. As discussed in previous work [9], such threshold values eliminate on the order of 95% of the false hits triggered by fluctuations in the baseline intensity (i.e. spectral noise), thereby optimizing the sensitivity to actual particle hits. This conditional data analysis scheme was performed in real-time for each 1200-shot sequence and the identified spectra for all particle hits were stored along with the ensemble-average of all laser pulses.

After each sampling period, the stored spectra of all identified particle hits for a given analyte species were ensemble-averaged and an equivalent mass concentration was calculated using calibration curves as discussed below. The equivalent mass concentration corresponds to the analyte signal strength as calculated using the subset of data identified with the conditional sampling algorithm. As such, the actual mass concentration of the ambient air sample is equal to the product of the equivalent mass concentration and the frequency of identified hits [28]. The frequency of hits is the number of spectra identified with the analyte peak present divided by the total number of laser pulses. It is noted that as the frequency of hits approaches 100%, the conditional analysis scheme converges to a traditional ensemble-averaging approach.

The quantitative analysis of LIBS data for particle size and composition measurements was presented in detail in a recent paper [9]. The technique is based on the relationship between the

equivalent mass concentration of a given analyte atomic emission peak, the analyte mass and the characteristic plasma volume. The equivalent mass concentration is calculated using a typical calibration curve relating the analyte LIBS signal to a known analyte mass concentration. All calibration curves used in this study were generated with well-controlled mass flow streams and were characterized by regression coefficients greater than 0.99. The LIBS signal in this study is defined as the integrated atomic emission line intensity normalized by the plasma continuum emission intensity adjacent to the emission line. As developed in the above-cited reference, the equivalent mass concentration is equal to the single particle mass divided by the plasma volume. Using this relationship, the equivalent spherical diameter of a single particle may be calculated using the expression:

$$D = \left[\frac{6xV_p}{\pi\rho f} \right]^{1/3} \quad (1)$$

where x is the equivalent mass concentration of the analyte species (mass/volume of gas), V_p is the characteristic plasma volume ($2.5 \times 10^{-4} \text{ cm}^3$), ρ is the overall particle density, and f is the mass fraction of the analyte with respect to the overall particle mass. For a homogeneous particle, f equals unity and ρ becomes the density of the analyte.

The algorithms discussed above enable the identification of spectra corresponding to individual particles, and the calculation of overall mass concentrations and the mass/size of individual particles. Two additional controls were added to the data reduction schemes. For mass concentration measurements, a total of two or more emission lines were utilized for each species. Typically, the most intense line was used to trigger the conditional data analysis routine. Then one or two additional lines were used to calculate the equivalent mass concentration based on the ensemble-averaged spectrum of the identified particle hits. As discussed in a previous paper [9], this approach prevents large spectral noise values that exceed the conditional analysis threshold criteria from contributing a false signal to the analyte

peak. Because the spectral noise is random on a given shot, a high noise spike on the analyte trigger wavelength would not correspond to high noise spikes on the alternative analysis wavelength or wavelengths. For single-shot analysis, comparing the analyte signal from two different atomic emission lines screens false noise or other spectral irregularities. A spectrum is rejected from subsequent single-shot size analysis if both atomic emission lines do not yield the same analyte mass to within a factor of 2. In other words, spectra are retained for size analysis only if the ratio of analyte masses calculated from two different emission lines is between 0.5 and 2.0.

All LIBS spectral data were collected and processed in real-time using a conditional data analysis routine to identify spectra corresponding to the targeted analyte species. All spectra corresponding to the presence of targeted analyte signals were stored and subsequently analyzed for particle size and mass composition. Three different spectral windows were utilized to monitor the species of interest. The three windows were centered at 275, 408 and 590 nm, with each having a spectral bandwidth of approximately 36, 32 and 25 nm, respectively, over the 1024-pixel intensified CCD detector array.

3. Results and discussion

Four elemental species were targeted for the ambient air monitoring reported in this paper, namely aluminum, magnesium, calcium and sodium. The corresponding atomic emission lines utilized were: the 394.40 and 396.15-nm Al I lines; the 279.55, 280.27 and 285.21-nm Mg I and II lines; the 393.37 and 396.85-nm Ca II lines; and the 589.00 and 589.59-nm Na I doublet. Aluminum and magnesium were selected because they are used as energetic fuels in many fireworks, while sodium and calcium were selected primarily as controls due to their general prevalence in atmospheric particulates. Data were analyzed for both overall mass concentrations and mass-based particle size.

An advantage of LIBS-based analysis of individual aerosol particles is the ability to determine

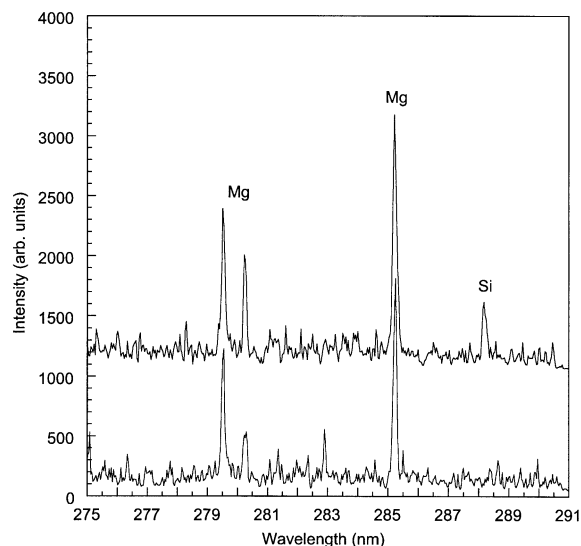


Fig. 3. Two single-shot LIBS spectra. The lower spectrum represents a single magnesium oxide particle. The upper spectrum, which has the same intensity scale but has been vertically shifted for clarity, represents a magnesium–silicate particle.

the composition of constituent elements within a given particle. Although the spectrometer/detector system used in the current study was limited to relatively narrow spectral bandwidths, several unique particle types, as observed by the combination of emission lines present, were identified during this study. Representative spectra are presented in Figs. 3 and 4. Fig. 3 contains two single-shot spectra corresponding to the spectral window centered around the magnesium emission lines. One spectrum is characterized by the presence of intense magnesium emission lines only, with no other emission features observed in the continuum. As discussed below, such a spectrum is attributed to a single MgO particle in this study. In contrast, the second spectrum features both magnesium and silicon (288.16-nm Si I) emission lines, and is attributed to a type of magnesium–silicate particle, for example uniformly composed MgSiO₃ or an agglomerate of MgO with a silicate particle. Such magnesium–silicate spectra were rare in comparison to the magnesium oxide spectra, with the latter accounting for greater than 95% of the recorded

magnesium-containing spectra. Fig. 4 contains two spectra corresponding to aluminum-containing particles, namely one spectrum containing only aluminum emission lines and a second spectrum characterized by the presence of both aluminum and calcium emission lines. Spectra characterized by the presence of both aluminum and calcium emission (e.g. aluminum calcite particle) accounted for less than 1% of the spectra containing calcium emission lines, and accounted for approximately 10% of the spectra containing aluminum emission lines. Particle size data are presented in detail below, however, the four spectra presented in Figs. 3 and 4 correspond to particle diameters in the range of 200–500 nm. The above data demonstrate the overall sensitivity of the LIBS technique for single particle analysis, as observed by the relative strength of the various atomic emission lines.

A novel feature of laser-induced breakdown spectroscopy is the ability to reject null spectral data while utilizing the infrequent but signal-rich spectra corresponding to discrete aerosol particles. The enhanced signal-to-noise ratio resulting

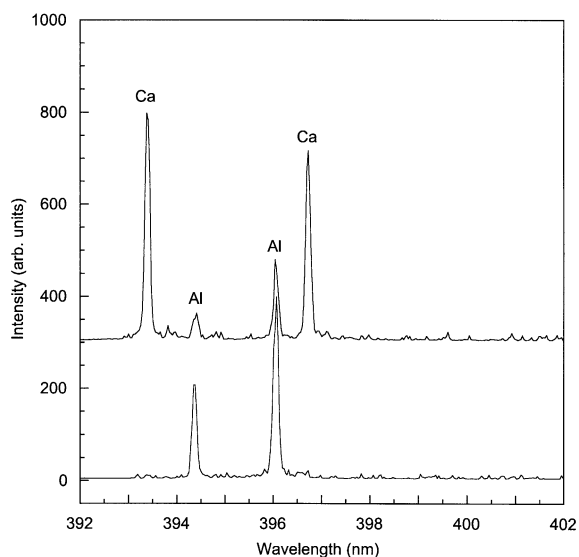


Fig. 4. Two single-shot LIBS spectra. The lower spectrum represents a single aluminum-containing particle. The upper spectrum, which has the same intensity scale but has been vertically shifted for clarity, represents a particle containing both aluminum and calcium.

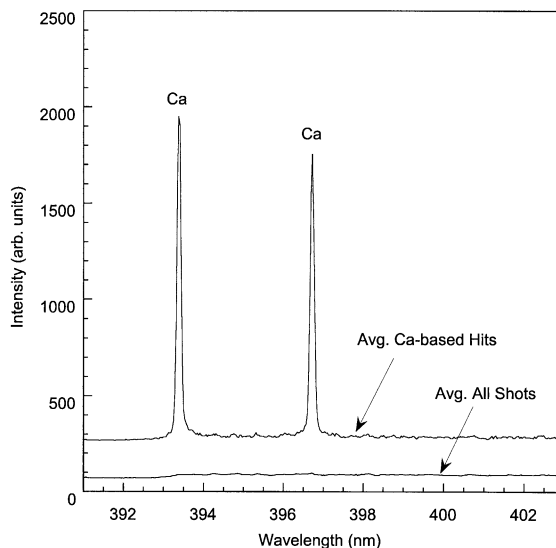


Fig. 5. LIBS spectra for calcium-based particle sampling. The lower spectrum corresponds to an ensemble average of 9600 laser pulses, and the upper spectrum corresponds to an average of 28 identified calcium-based particle hits from the 9600 laser shots. Both spectra have the same intensity scale but have been vertically shifted for clarity.

from the conditional analysis-based LIBS monitoring is illustrated in Fig. 5 for calcium-based particle sampling. The figure presents the spectrum corresponding to the ensemble-average of data for all laser pulses along with the corresponding spectrum based on the ensemble-average of data for identified particle hits only. The calcium data presented in Fig. 5 correspond to the morning of July 7, with the lower spectrum based on the average of 9600 laser pulses and the upper spectrum corresponding the subset of 28 spectra recorded for calcium particle hits. The corresponding calcium-based particle sampling frequency is 28/9600 or approximately 0.3% of laser pulses. The increase in analyte signal-to-noise ratio is very significant, with the 9600-shot ensemble-average essentially equal to a non-detectable calcium emission signal. The effective mass concentration of the calcium hits spectrum is approximately 137 parts per billion (ppb; mass calcium/mass air), while the overall calcium concentration is $137 \times (0.3/100)$ or approximately 0.4 ppb. The nominal improvement in signal-to-noise

ratio is approximately 2 orders of magnitude for this calcium sampling frequency, which is apparent in the Fig. 5 spectra. Sodium-containing emission spectra revealed similar enhancement in sodium emission line intensity with the use of conditional data analysis.

As illustrated above, the use of a conditional data analysis routine yields spectra with excellent signal-to-noise ratios for the observed ambient air particle sampling rates. The spectral data were subsequently used to calculate overall mass concentration measurements of aluminum, calcium, magnesium and sodium throughout the sample period. The mass concentration of magnesium recorded in ambient air is presented in Fig. 6 as a function of time. The mass concentration ranged from 0 to 108 parts per trillion (ppt) on a mass basis. It is noted that 1 part per trillion on a mass basis is equivalent to 1.16 ng/m^3 of ambient air. A mass concentration of zero corresponds to a sampling frequency of zero or an equivalent mass concentration of the particle hits less than 10 parts per billion, the lower detection limit established for magnesium for the spectra corresponding to the particle hits. The magnesium-based particle sampling rates were typically 0.1% or less; hence the actual analyte signals corresponding to the Fig. 6 data were approximately 3 orders of magnitude larger than the overall mass concentration values. The data presented in Fig. 6 reveal a significant rise in magnesium during the Fourth of July holiday period, considered to span from July 1 to July 7 as discussed above. The average magnesium concentration during the holiday period was 44.5 ppt, with a high of 108 ppt, while the average concentration of magnesium before and after the holiday period was 0 and 3.6 ppt, respectively. The nearly 50-fold increase in magnesium during the Fourth of July holiday period in comparison to the average of pre- and post-holiday concentrations is strongly suggestive that the source of increased magnesium is derived from the discharge of fireworks in the troposphere. The mass concentration data recorded for aluminum during the same sampling period revealed trends similar to the magnesium data. However, the overall aluminum-sampling hit rates were significantly lower than the magnesium sam-

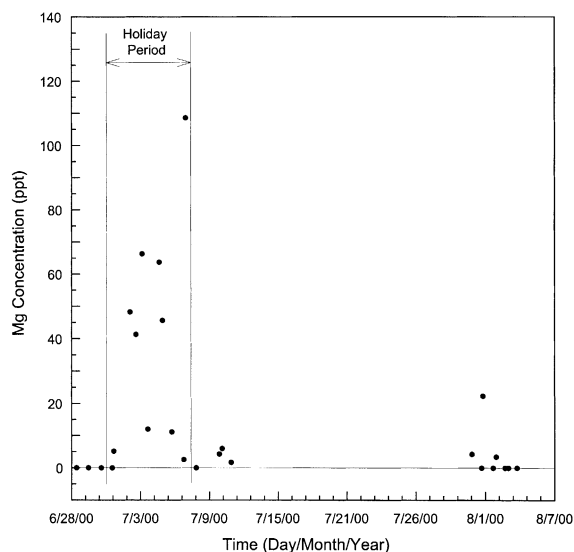


Fig. 6. Mass concentration of magnesium as a function of time. Each data point represents the average LIBS-based concentration over a 2-h sampling period.

ple rates. As such, the aluminum data contained a larger percentage of zero concentration measurements, essentially non-detects. The average aluminum concentration was 46 ppt during the holiday period, compared to an average mass concentration of 7 ppt before and after the holiday period. The current findings of increased magnesium and aluminum are consistent with results reported during a similar study that utilized laser desorption/mass spectrometry for the analysis of ambient air particles [31]. The study reported significant increases in the levels of ambient air magnesium and other elements attributed to fireworks in the days following the Fourth of July holiday at the University of California in Riverside. Although the total masses of magnesium and aluminum released by fireworks are diluted with a significant volume of ambient air, the current study and the work of Liu et al. [31] suggest that pyrotechnic-derived particulates persist in the troposphere with a time scale on the order of days.

The mass concentration data for calcium and sodium are presented in Fig. 7 for the same time period. In contrast to the magnesium and aluminum data, the mass concentrations of cal-

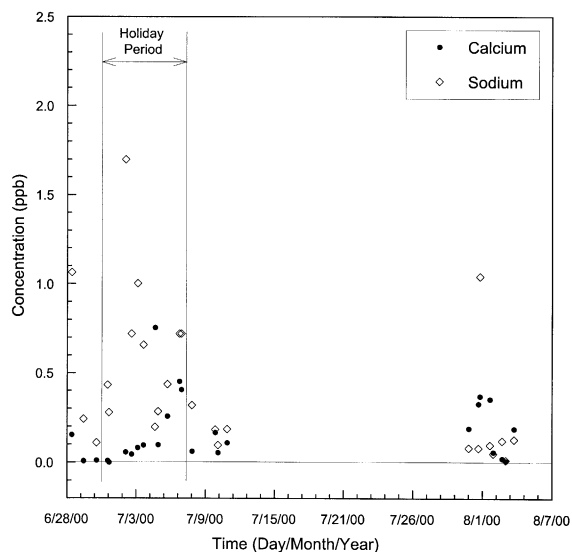


Fig. 7. Mass concentrations of calcium and sodium as a function of time. Each data point represents the average LIBS-based concentration over a 2-h sampling period.

cium and sodium do not correlate as strongly with the Fourth of July holiday period. The average calcium and sodium concentrations during the holiday period were 0.21 and 0.65 parts per billion (ppb) by mass, respectively, while the pre- and post-holiday average calcium and sodium concentrations were 0.14 and 0.25 ppb, respectively. Although sodium and calcium may be a component of select fireworks, the prevalence of both calcium and sodium is well documented in ambient air under normal conditions [32–36]. It is difficult to determine the contribution of fireworks-derived calcium and sodium to the recorded mass concentrations due to the relatively large background levels and daily fluctuations of these species. For example, the standard deviations ($n - 1$) of the measured sodium mass concentration data are equal to 0.43 and 0.33 ppb, corresponding to the holiday and non-holiday sampling periods, respectively. The difference between holiday and non-holiday sodium concentrations (approx. 0.4 ppb) is within the standard deviations for these two sample sets, making it difficult to conclude any statistical significance to the fluctuations in sodium and calcium over the Fourth of July holiday. The maximum mass concentration

of sodium was 1.7 ppb, recorded on the evening of July 2, while the maximum calcium mass concentration was 0.75 ppb recorded on the morning of July 5. The ambient air concentrations of calcium and sodium were greater by approximately 2 orders of magnitude in comparison to magnesium and aluminum values. No independent sampling and analysis techniques were used to corroborate the reported mass concentration data. However, in an earlier study, independent extractive sampling in accordance with US EPA Method 29 standards yielded excellent agreement for chromium and manganese concentration measurements at 2–3 ppb mass concentrations [28]. In aggregate, the current mass concentration data demonstrate the ability of the LIBS technique to measure element-specific concentrations of particulate matter at very low overall mass concentration levels.

While the mass concentration data presented above are based on conditional data analysis corresponding to approximately 2-h sampling periods, it also useful to examine the data with finer temporal resolution. The sampling frequencies of recorded sodium-based particle hits based on individual 1200-shot laser sequences (i.e. 4-min sequences) are presented in Fig. 8 for the 2-h

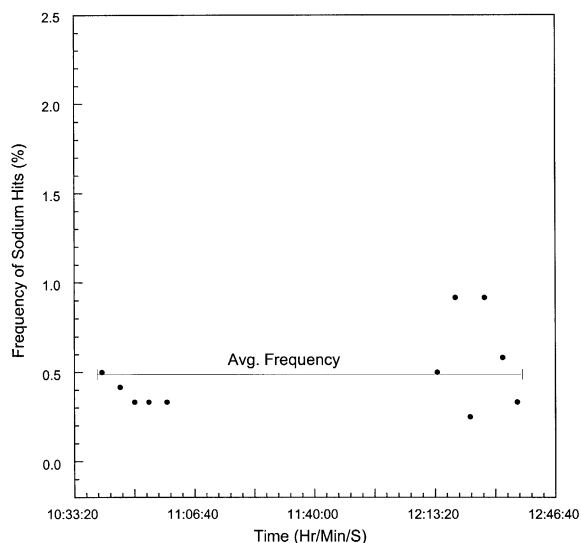


Fig. 8. Sampling frequency of sodium-based particle hits over a 2-h period on July 4. Each data point corresponds to the frequency of sodium hits for a 1200-shot laser sequence.

sampling period monitored on the morning of July 4. The 4-min sampling frequencies of sodium-based particles ranged from 0.25 to 0.92% during this 2-h period, which corresponds to a factor of 2 within the average sampling rate of 0.49%. The time-resolved sampling data presented in Fig. 8 are typical of the relatively steady nature of particulate matter observed on the time scale of minutes to several hours. Additional studies will focus on the temporal variations in ambient air particulates and the resolution of the LIBS technique for monitoring such phenomena.

In addition to the evaluation of mass concentrations, the individual spectra corresponding to each particle hit were analyzed for elemental mass and subsequent particle size. As outlined in detail in a recent paper [9], the LIBS-based measure of elemental mass within a single particle may be used to infer the particle size. The elemental mass is directly calculated from the product of the equivalent analyte mass concentration of a single-shot spectrum and the characteristic plasma volume. For this study, the characteristic plasma volume was $2.5 \times 10^{-4} \text{ cm}^3$ as reported previously [29]. As observed in Eq. (1), the calculation of a mass-based particle diameter requires the specification of parameters based on the particle type, namely the bulk particle density and the elemental mass fraction of the measured analyte species.

For the present study, the magnesium-based particles were modeled as magnesium oxide, MgO, with a density of 3.58 g/cm^3 and a magnesium mass fraction of 0.60. MgO was utilized as a model based on several observations, including the perceived particle source of magnesium, namely via combustion-generation during the discharge of fireworks. As noted above, nearly all of the magnesium particles were characterized by the absence of any recorded silicon or iron atomic emission lines. Furthermore, modeling the particles as sea salt-based particles, which contain significant fractions of magnesium, was discounted for the magnesium-based particles due to the mass values of magnesium and sodium recorded. The Na/Mg mass ratio for sea-salt particles is nominally 7.8 [36], which is not consistent with the present calculated values. Specifi-

cally, the average mass of particulate magnesium was 24 femtograms (fg), while the average mass of particulate sodium was 30 fg, with a corresponding Na/Mg ratio of only 1.25. Although the largest recorded sodium particle mass is consistent with the nearly 8:1 Na/Mg ratio, the recorded sampling frequency of the largest sodium particles is inconsistent with the recorded sampling frequency of magnesium particles. Simultaneous monitoring of both sodium and magnesium emission lines would remove the ambiguity associated with magnesium and sodium-containing particles, and is a goal of future research.

The calcium particles were modeled as calcium carbonate, CaCO_3 , with a density of 2.71 g/cm^3 and a calcium mass fraction of 0.40. Calcium in ambient air particulates is mostly composed of calcium carbonate or gypsum [34], although CaSO_4 particulates from anthropogenic sources may be significant in number [33]. The sodium particles were modeled as two different particle types, namely sodium chloride, with a density of 2.17 g/cm^3 and a sodium mass fraction of 0.39, for particles with a corresponding mass-based diameter less than $1 \text{ }\mu\text{m}$, and sodium nitrate for particles greater than $1 \text{ }\mu\text{m}$. Such a categorization is consistent with recent measurements reported of nitrate-containing particles using an aerosol time-of-flight spectrometer [37]. Specifically, sodium nitrate particles were limited to the coarse size mode between 1 and $3.5 \text{ }\mu\text{m}$. Deviations in the ratio of Cl/Na from reference seawater values have been reported for submicrometer sea-salt aerosols [36], although no attempt was made in this study to account for chlorine depletion. In a recent study, LIBS-based size measurements were recorded for laboratory generated aerosols modeled as calcium and magnesium hydroxides, which were in excellent agreement with independent light-scattering based size measurements [9].

The histogram of calculated diameters (as MgO) for the magnesium-containing particles recorded during the Fourth of July holiday period is presented in Fig. 9. The mean diameter is 276 nm, with a standard deviation of 93 nm. The size distribution exhibits a skewness toward larger particle sizes, as expected for general aerosol populations. The mean particle size of magne-

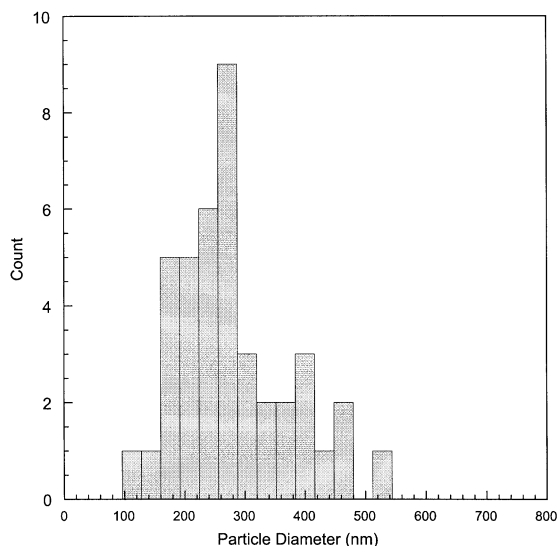


Fig. 9. Histogram of calculated diameters for magnesium-containing particles for the Fourth of July holiday period. The particles were modeled as magnesium oxide (MgO).

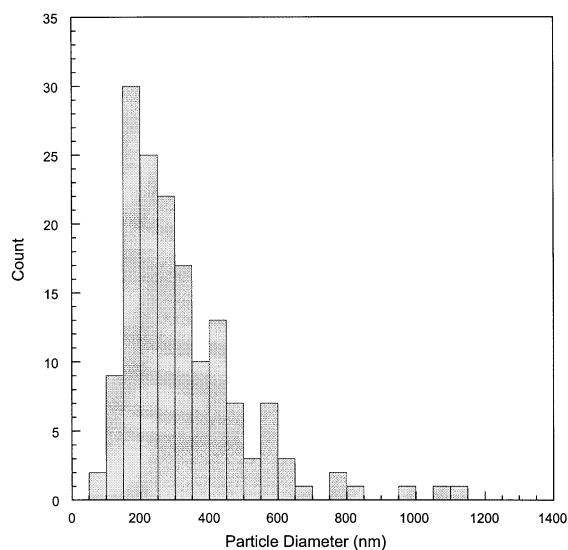


Fig. 10. Histogram of calculated diameters for calcium-containing particles for the Fourth of July holiday period. The particles were modeled as calcium carbonate (CaCO_3).

sium-based particles recorded after the holiday period was 206 nm, with a standard deviation of 83 nm. The approximately 70-nm difference in mean diameters, approximately a 25% decrease, between the sizes of these two magnesium-based particle populations is not statistically significant, but nonetheless may be indicative of two different sources of magnesium particles, namely fireworks derived and perhaps marine-derived. In contrast, the calcium and sodium particle size distributions revealed essentially no variations with respect to the holiday period. The size distribution recorded for the calcium particles (as CaCO_3) is presented in Fig. 10. The mean particle diameter is 323 nm with a standard deviation of 180 nm, and with a modal diameter of approximately 175 nm. A long tail is extended toward the larger diameters, with a maximum-recorded diameter of approximately 1.1 μm . The largest particles have a calcium mass approximately 250 times larger than the mass associated with the modal particle diameter. The size distribution of pre- and post-holiday calcium-based particles was essentially identical to the Fig. 10 data. The mean diameter and standard deviation were 330 and 173 nm, respectively, which are within 1% of the particle values

recorded during the holiday period. For comparison, the cumulative probabilities of the two calcium-based particle size distributions are plotted in Fig. 11. The similar curves in Fig. 11 are consistent with the previous discussion regarding particulate calcium not being associated appreciatively with the discharge of fireworks.

The histogram of submicron-sized sodium par-

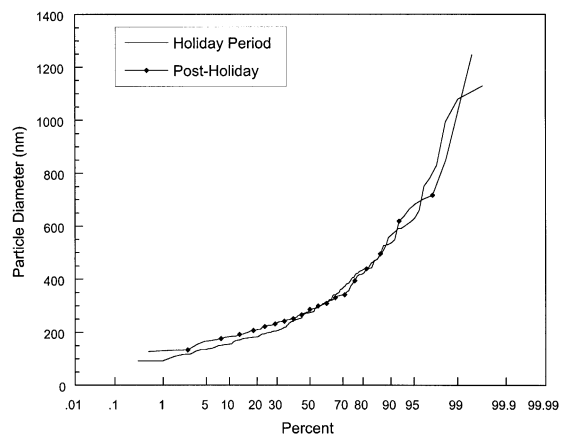


Fig. 11. Cumulative probabilities of calcium-based particle diameters both for the holiday period and the post-holiday period.

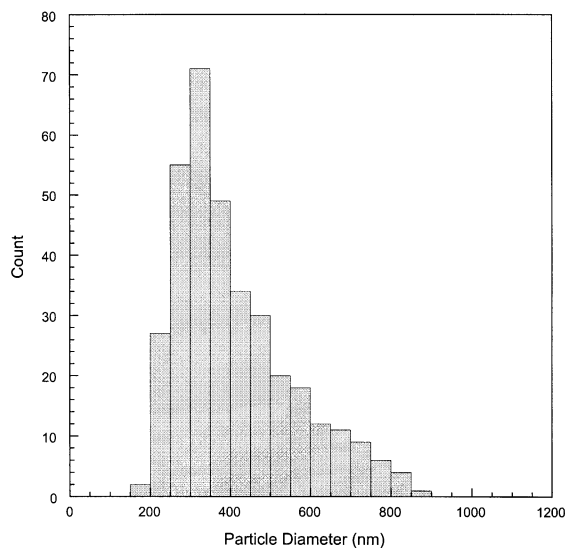


Fig. 12. Histogram of calculated diameters for submicron-sized sodium-containing particles for the Fourth of July holiday period. The particles were modeled as sodium chloride (NaCl).

ticles (as NaCl) is presented in Fig. 12 for the holiday period. The mean and modal particle diameters are approximately 410 and 325 nm, respectively, with a standard deviation of the distribution equal to 144 nm. As with the calcium results, the non-holiday associated sodium particles were consistent with the size distributions recorded during the holiday period. Specifically, the mean and standard deviation of the post-holiday sodium-based particles were 387 and 117 nm, respectively. As discussed above, the sodium-based particles larger than $1 \mu\text{m}$ were modeled as sodium nitrate. The sodium nitrate particles accounted for approximately 3% of the sodium-based particle hits recorded, and were characterized by an equivalent size that ranged between 1.1 and $1.9 \mu\text{m}$.

It is also useful to discuss the absolute detectable analyte masses and the relative sensitivity of the LIBS technique for the species analyzed in this paper. The smallest particle diameters reported in Figs. 9 and 10 and Fig. 12 represent the minimum detected masses of magnesium, calcium and sodium, respectively. Because the probability is low that the actual ambient air size distributions naturally ended at these points, these

minimum detected sizes are considered representative of the analyte mass detection limits. For calcium, magnesium and sodium, the minimum detected masses were 0.5, 1.2 and 3.3 femtograms, respectively, with corresponding particle diameters of approximately 90, 100 and 195 nm. It is noted that particle size modes on the order of tens of nanometers may exist for select particle types (i.e. combustion derived). At present such nanoparticles are not detectable as single particles using LIBS as implemented in the present study. An additional parameter that should be noted is the rate of acceptance of the single-shot spectra. As detailed above, the criteria for analysis of a single-shot spectrum was that the calculated analyte mass was consistent (within a factor of 2) for two atomic emission lines. The retention rate for the spectra of sodium-based particles was 90%, and the retention rates were 63 and 50% for the spectra of calcium and magnesium-based particles, respectively. These rates reflect a number of factors including: the overall LIBS sensitivity to each analyte emission line; the signal-to-noise ratio in the various spectral regions; and the specific nature of the emission line pairs (e.g. neutral line to ionic line as with magnesium). Single-shot variations in atomic emission spectra in consideration with plasma properties are the focus of ongoing work.

4. Conclusions

The LIBS technique was successfully used to monitor ambient air particulates containing a number of species. Data were analyzed both for overall mass concentrations and for mass and size measurements of individual particles. A conditional data analysis algorithm was implemented in real-time to identify spectra corresponding to individual aerosols. This approach was successful in increasing the signal-to-noise ratios by rejecting null spectral data. For the relatively low aerosol loadings observed, nominal increases in analyte signal were approximately 2–3 orders of magnitude with conditional data analysis. The Fourth of July holiday period provided a unique sampling opportunity to record significant changes in am-

bient air concentrations of metallic species associated with the discharge of fireworks in the troposphere. Order-of-magnitude increases in magnesium and aluminum mass concentrations were observed during the holiday period, and were attributed directly to the discharge of fireworks. In contrast, recorded ambient air concentrations of sodium and calcium revealed no significant correlation with the Fourth of July holiday period. Temporal data were also examined, thereby demonstrating the ability of the LIBS technique to monitor ambient air particulate matter with a temporal resolution of a few minutes.

The LIBS technique is well suited for the unique problem of aerosol analysis because of the ability to couple a small sample volume with single-shot analysis, thereby taking advantage of the discrete analyte mass associated with individual particles. Ambient air mass concentration measurements were recorded for magnesium and aluminum as low as one part per trillion. The absolute mass detection limits for single particle analysis exceeded sub-femtogram values for calcium-containing particles, and was on the order of 2–3 femtograms for magnesium and sodium-based particles. Overall, the LIBS technique is promising for the challenging issues associated with the real-time collection and analysis of ambient air particulate matter data. The use of advanced spectrometer systems, such as echelle designs, with a broader spectral bandwidth will enable a greater amount of species-to-species correlations.

Acknowledgements

This work was supported in part by the US Department of Energy and the US Department of Defense, Joint Services Demil Technology Office, in conjunction with Sandia National Laboratories, Livermore, CA.

References

- [1] A. Wexler, K. Prather, *Aerosol Sci. Technol.* 33 (2000) 1–2.
- [2] U.S. Environmental Protection Agency, Federal Register 61, 77, (1996) 17357–17358.
- [3] U.S. National Research Council, *Research Priorities for Airborne Particulate Matter: II. Evaluating Research Progress and Updating the Portfolio*, (1999).
- [4] K.A. Prather, T. Nordmeyer, K. Salt, *Anal. Chem.* 66 (1994) 1403–1407.
- [5] J.T. Jayne, D.C. Leard, X. Zhang, P. Davidovits, K.A. Smith, C.E. Kolb, D.R. Worsnop, *Aerosol Sci. Technol.* 33 (2000) 49–70.
- [6] P.G. Carson, M.V. Johnston, A.S. Wexler, *Rapid Commun. Mass Spectrom.* 11 (1997) 993–996.
- [7] H.J. Tobias, P.M. Kooiman, K.S. Docherty, P.J. Ziemann, *Aerosol Sci. Technol.* 33 (2000) 170–190.
- [8] W.D. Reents, *Z. Ge. Aerosol Sci. Technol.* 33 (2000) 122–134.
- [9] D.W. Hahn, M.M. Lunden, *Aerosol Sci. Technol.* 33 (2000) 30–48.
- [10] M.D. Seltzer, G.A. Meyer, *Environ. Sci. Technol.* 31 (1997) 2665–2672.
- [11] M.D. Seltzer, R.B. Green, *Process Control Qual.* 6 (1994) 37–46.
- [12] P.P. Woskov, D.Y. Rhee, P. Thomas, D.R. Cohn, J.E. Surma, C.H. Titus, *Rev. Sci. Instrum.* 67 (1996) 3700–3707.
- [13] Y.X. Duan, Y.X. Su, Z. Jin, S.P. Abeln, *Anal. Chem.* 72 (2000) 1672–1679.
- [14] S.A. Darke, J.F. Tyson, *J. Anal. At. Spectrom.* 8 (1993) 145–209.
- [15] L.J. Radziemski, *Microchem. J.* 50 (1994) 218–234.
- [16] D.A. Rusak, B.C. Castle, B.W. Smith, J.D. Winefordner, *Crit. Rev. Anal. Chem.* 27 (1997) 257–290.
- [17] I. Schechter, *Rev. Anal. Chem.* 16 (1997) 173–298.
- [18] K. Song, Y.I. Lee, J. Sneddon, *Appl. Spectrosc. Rev.* 32 (1997) 183–235.
- [19] M.Z. Martin, M.D. Cheng, R.C. Martin, *Aerosol Sci. Technol.* 31 (1999) 409–421.
- [20] J. Sneddon, Y.I. Lee, *Anal. Lett.* 32 (1999) 2143–2162.
- [21] R.E. Neuhauser, U. Panne, R. Niessner, *Anal. Chim. Acta* 392 (1999) 47–54.
- [22] D.K. Ottesen, J.C.F. Wang, L.J. Radziemski, *Appl. Spectrosc.* 43 (1989) 967–976.
- [23] I. Schechter, *Anal. Sci. Technol. (J. Korean Soc. Anal. Sci.)* 8 (1995) 779–786.
- [24] L.W. Peng, W.L. Flower, K.R. Hencken, H.A. Johnsen, R.F. Renzi, N.B. French, *Process Control Qual.* 7 (1995) 39–49.
- [25] J.P. Singh, F.Y. Yueh, H. Zhang, R.L. Cook, *Process Control Qual.* 10 (1997) 247–258.
- [26] S.G. Buckley, H.A. Johnsen, K.R. Hencken, D.W. Hahn, *Waste Manage.* 20 (2000) 455–462.
- [27] R.E. Neuhauser, U. Panne, R. Niessner, P. Wilbring, *Fresenius J. Anal. Chem.* 364 (1999) 720–726.
- [28] D.W. Hahn, W.L. Flower, K.R. Hencken, *Appl. Spectrosc.* 51 (1997) 1836–1844.
- [29] D.W. Hahn, *Appl. Phys. Lett.* 72 (1998) 2960–2962.
- [30] A. McFarland, *Deposition Version 4.0*, Texas A and M University, College Station, TX, 1996.

- [31] D.Y. Liu, D. Rutherford, M. Kinsey, K.A. Prather, *Anal. Chem.* 69 (1997) 1808–1814.
- [32] P.H. McMurry, M. Litchy, P.F. Huang, X.P. Cai, B.J. Turpin, W.D. Dick, A. Hanson, *Atmos. Environ.* 30 (1996) 101–108.
- [33] S. Hoornaert, H. Van Malderen, R. Van Grieken, *Environ. Sci. Technol.* 30 (1996) 1515–1520.
- [34] P. Laj, G. Ghermandi, R. Cecchi, V. Maggi, C. Riontino, S.M. Hong, J.P. Candelone, C. Boutron, *J. Geophys. Res. Oceans* 102 (1997) 26615–26623.
- [35] D.S. Lee, G.J. Dollard, R.G. Derwent, S. Pepler, *Water Air Soil Pollut.* 113 (1999) 175–202.
- [36] L.M. McInnes, D.S. Covert, P.K. Quinn, M.S. Germani, *J. Geophys. Res. Atmos.* 99 (1994) 8257–8268.
- [37] D.Y. Liu, K.A. Prather, S.V. Hering, *Aerosol. Sci. Technol.* 33 (2000) 71–86.